Design Considerations in Optical Add/Drop Multiplexers Based on Grating-Assisted Null Couplers

Christos Riziotis and Mikhail N. Zervas

***Abstract*—The performance of a fully optimized optical add/drop multiplexer (OADM), based on null couplers and tilted Bragg gratings, is studied in detail. It is shown that maximization of the device performance involves three main optimization steps. First, the waveguide asymmetry (V_2/V_1 ratio) should be optimized in order to minimize the extinction ratio of the unwanted mode at the null coupler waist. Second, the coupler taper shape should be optimized in order to further minimize the aforementioned extinction ratio. Third, the grating tilt angle and relative width can be also optimized to give negligible backreflections at the input port and minimize radiation losses. The results show that the proposed high-performance OADM configuration can meet the stringent telecom specifications.**

***Index Terms*—Gratings, null couplers, optical add/drop multiplexers (OADMs), tilted gratings, wavelength division multiplexed (WDM) transmission.**

I. Introduction

ONE OF THE most critical components for the developing technology of wavelength-division multiplexed (WDM) systems is the optical add/drop multiplexer (OADM). A very simple four-port device that adds and/or drops a particular channel can serve as building block of a more complicated system. Simple OADM configurations, using the unique spectral characteristics of phase Bragg gratings, appear to be quite promising solutions intended to find applications in high-performance WDM systems.

A number of different four-port OADM configurations have been proposed. The simplest one, which makes direct use of the reflection properties of a Bragg grating written in a single mode fiber, is the well-known configuration with the two optical circulators (OCs) [1]. This OADM implementation is frequently used as a benchmark in the sense that it provides excellent crosstalk performance and negligible back reflections. In addition, the reflection and dispersion characteristics of the OADM are identical to the ones of the grating. However, it should be stressed that because of the circulators this OADM suffers from relatively high insertion loss (~1 dB), it is bulky and expensive and cannot be easily integrated.

Manuscript received May 15, 2000; revised October 2, 2000. This work was supported in part by the UK EPSRC project PHOTON. The Optoelectronics Research Centre is an EPSRC-funded Interdisciplinary Research Centre.

C. Riziotis is with the Optoelectronics Research Centre, University of Southampton, Southampton SO17 1BJ, U.K. (e-mail: cr@orc.soton.ac.uk).

M. N. Zervas is with the Optoelectronics Research Centre, University of Southampton, Southampton SO17 1BJ, U.K., and also with Southampton Photonics, Ltd., Southampton, U.K.

Publisher Item Identifier S 0733-8724(01)00404-2.

More compact grating-based OADMs, without the use of circulators, can be classified in two main categories, namely, interferometric and noninterferometric. Interferometric OADMs rely on the interference between two optical signals reflected by Bragg gratings that are incorporated into various interferometric optical arrangements, such as Mach–Zehnder interferometers (MZIs) [2]–[7] and symmetric, full (100%) couplers (SFCs) [8]–[10]. A perfectly matched MZI-based OADMs, with identical gratings in each arm, can potentially result in an ideal performance, better than the one of OC-based OADMs, since they show no backreflections and need no extra components, i.e., circulators or isolators. Additionally they can provide very low insertion losses (~0.1 dB) and they can be fully integrated. However, grating mismatches and interferometer-arm imperfections compromise the OADM performance severely, resulting in strong backreflections and spectral distortions. In his case, careful post-processing and trimming is required. In addition, two extra isolators are quite likely to be required at the two input ports to avoid the deleterious effects of backreflections, making the total extra-component count equal to the OC-based devices. In the SFC-based OADMs, on the other hand, the grating is placed in the coupler waist to reflect the two lowest-order eigenmodes. These modes, however, have different propagation constants and the corresponding reflected spectra are always partially overlapping [11]. This results always in partial interference and produces strong backreflections and spectral distortions and, as before, two extra isolators might be needed. On the other hand, the grating has to be placed precisely in the correct position for optimum operation [10].

The third general category of OADMs includes those based on grating assisted-contradirectional coupling in asymmetric couplers [12]–[16]. In this case, a grating is used to contradirectionally couple light between two otherwise dissimilar uncoupled waveguides. In this geometry there are, in general, three types of interactions involving *even–even* (e–e), *odd–odd* (o–o) eigenmode self-coupling, as well as *even–odd* (e–o) eigenmode resonant cross-coupling. This results in a maximum of three reflection peaks appearing in the drop- and add-port spectra, as well as, strong backreflections in the input port. The relative strength of these peaks can be controlled by careful grating design. In one configuration, the grating is formed in only one of the cores of a dual dissimilar-core fiber to minimize backreflections [14]. An extensive theoretical analysis of this device, discussing all the optimization steps and design compromises, has been recently published by Erdogan [17].

0733–8724/01$10.00 © 2001 IEEE

Authorized licensed use limited to: UNIVERSITY OF SOUTHAMPTON. Downloaded on October 7, 2009 at 07:15 from IEEE Xplore. Restrictions apply.

Finally, another noninterferometric OADM configuration (see Fig. 1), based on a null coupler with a tilted grating in its waist, has been recently reported by Kewitsch *et al.* [15]. Null couplers are comprised of two dissimilar waveguides brought gradually in close proximity and finally in contact to form the waist. The devices are actually based on adiabatic mode transformation [18], [19] taking place along the coupler arms and their waist. A short period UV-written tilted grating can provide resonant contra-directional coupling and add/drop function [15]. The principle of operation of the device is discussed in more detail in Section II. A nonoptimized null coupler device, however, will exhibit the same performance limitations as the other devices of this category, namely, a maximum of three reflection peaks at the drop- and add-port spectra, as well as, strong backreflections at the input port. In addition to OADMs, null couplers have also been excited with propagating flexural acoustic waves and successfully used for the implementation of other high-quality fiber components, such as frequency shifters and switches [18], [19].

In this paper, we present a detailed theoretical analysis of the null-coupler OADM and investigate the conditions and design requirements for fully optimized operation. The proposed optimization process [20] involves two main steps, namely, 1) the null-coupler and 2) the tilted-grating designs. In the first step, the branch V-number asymmetry and the taper-region shape are optimized in order to obtain pure mode transformation. In the second step, the grating tilt-angle and transverse extent are optimized in order to maximize even–odd mode conversion and at the same time minimize the resulted backreflections.

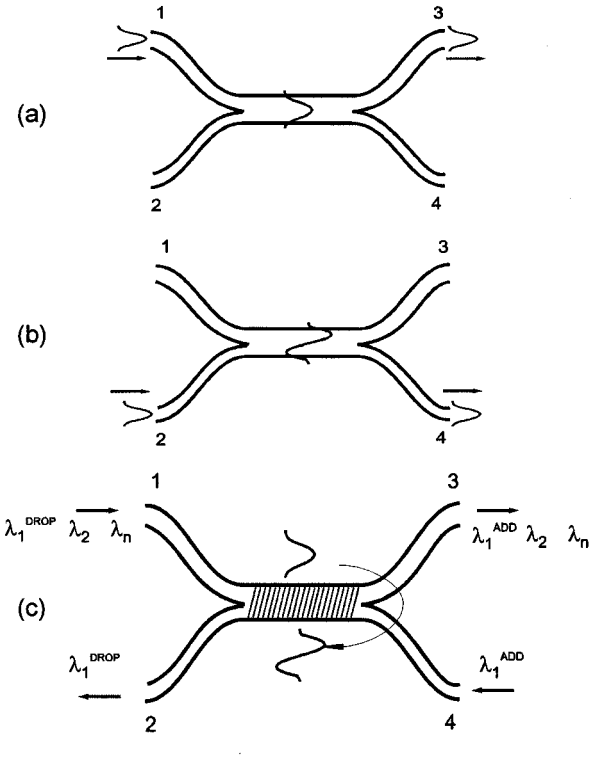

Fig. 1. Schematic of the OADM based on grating-assisted mode conversion in a null coupler. (a) Propagation of the even mode along the coupler. (b) Propagation of the odd mode along the coupler. (c) Cross-coupling of the two waist eigenmodes and demonstration of the OADM operation.

II. Principle of Operation

The schematic of the proposed OADM device is shown in Fig. 1. As mentioned already, null couplers are comprised of two dissimilar single-mode waveguides that are brought gradually in close proximity to form the waist. The devices are first relying on the adiabatic mode transformation that takes place along the coupler arms and waist. Light launched in one of the ports excites predominantly *only one* of the waist eigenmodes, which, in the absence of any perturbation, appears uncoupled at the output side of the same waveguide. Actually, light from the larger V-number input waveguide (e.g., port 1) excites only the *even lowest-order* (fundamental) mode at the coupler waist [see Fig. 1(a)] and proceeds uncoupled at the output of the waveguide with the same V-number (i.e., port 3). Similarly, light from the smaller V-number input waveguide (e.g., port 2) excites only the *odd lowest-order* mode at the coupler waist [see Fig. 1(b)] and proceeds uncoupled at the output of the waveguide with the same V-number (i.e., port 4). Strictly speaking, under normal circumstances, the null coupler (as the name implies) *does not* couple light. The mode transformation should be kept adiabatic all along to avoid extra radiation losses and unwanted mode excitation. In the presence, however, of an asymmetric periodic index perturbation along the coupler waist, power from one eigenmode can be resonantly transferred into the other one and finally appear at the opposite waveguide [see Fig. 1(c)]. The grating parameters, such as period and tilt, determine which one of the channels launched into port 1 will be dropped into port 2. The rest of the channels, of course, will be transmitted at port 3. Similarly, a channel at the Bragg wavelength launched into port 4 will be added into the transmission port 4.

The performance of the OADM depends critically on a number of factors. First, the waveguide asymmetry and coupler taper region should be optimized in order to maximize the excitation of the required eigenmode and eliminate the presence of the unwanted forward-propagating eigenmode at the waist. Second, the grating tilt and extend in the coupler waist should also be optimized in order to maximize the cross-coupling and energy transfer between forward even (odd) and backward odd (even) modes for efficient drop and add functions. In addition, even–even and odd–odd interactions and self-coupling should be minimized to avoid backreflections into the input port.

III. Null Coupler Design and Optimisation

The design of a high-performance null coupler involves two main optimization steps; namely, 1) coupled-waveguide asymmetry and 2) coupler taper shape. In this section, we briefly describe the basic theory used for the analysis of the asymmetric coupled structure and coupler taper region, as well as, the variational procedure for determining the optimum taper shape. The model is then used to design a fully optimized coupler.

Authorized licensed use limited to: UNIVERSITY OF SOUTHAMPTON. Downloaded on October 7, 2009 at 07:15 from IEEE Xplore. Restrictions apply.

A. Step-Wise Approximation of Null Coupler

For the analysis of the coupler, we used the local normal-mode analysis and the step-transition model [21], [22]. All the calculations are based on a general five-layer planar structure with step refractive index profiles. Despite its simplicity, this model provides a deep physical insight into the mechanisms of mode conversion, which are important for the understanding of the operation of null couplers and general grating-assisted filters. The normal mode analysis takes directly into account the physical shape of the coupler allowing us to optimize the performance of a null coupler by finding suitable branch shapes.

The continuous coupler structure is approximated by a series of discontinuous abrupt steps, separated by regions of parallel, five-layer waveguide (see Fig. 2). Light launched into one of the input ports is propagated through the coupler by expressing it in terms of the local coupled-structure eigenmodes. Local normal modes propagate in straight segments without any amplitude changes, experiencing only phase changes. Coupling between local normal modes of different segments takes place only at each step. By dividing the structure into a large number of small steps and repeating this process at each step a reasonable approximation of the mode's evolution is obtained. In isolation, each individual waveguide is single-mode and, therefore, the coupled structure supports two propagating (even and odd) eigenmodes.

Throughout the analysis, we consider TE polarized light only. The electric field guided orthonormal eigenmodes can be written as

$$e_y(x, z) = A(i) \cdot \Psi_\beta(x, z) \exp(-j \cdot a(z)),$$
$$a(z) = \beta(i) z + \varphi \tag{1}$$

where

- $A(i)$ normalized amplitude;
- $\Psi_{\beta(i)}(x, z)$ electric modal field distribution;
- $\beta(i)$ corresponding propagation constant of the ith eigenmode ($i = 1, 2$ for even and odd modes, respectively);
- φ arbitrary phase constant.

At each step along the structure, the propagation constants of the normal modes are obtained from the solutions of the corresponding characteristic equation [22].

The propagation algorithm consists of a group of iterative equations [21] that estimate at each step, the normalized amplitude and the phase of the propagating normal modes, based on the values from the previous step. Fig. 3 shows the basic coupler configuration and summarizes the main geometric and optical parameters used in the calculations.

B. Waveguide Asymmetry Optimization

The coupler performance is characterized by the power crosstalk, defined as the ratio $P_4/(P_3 + P_4)$ where P_3 and P_4 are the powers at the output ports 3 and 4, respectively, when the coupler is excited from port 1. Given that the reflective grating is placed in the null-coupler waist, in order to study the effect of waveguide asymmetry on the null coupler performance, it is better to reduce the problem to the study of an asymmetric Y-branch. We first consider taper regions with linearly shaped branches. Fig. 4 shows the crosstalk $P_2/(P_1 + P_2)$ variation as a function of the width of one of the waveguides, for two

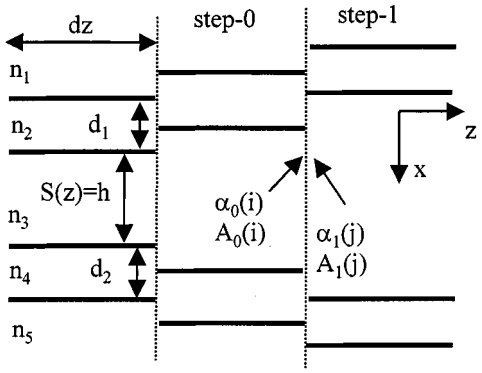

Fig. 2. Schematic of the step transition model.

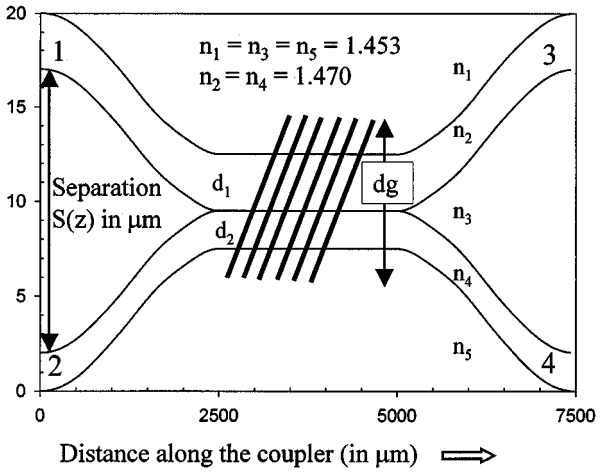

Fig. 3. Schematic and parameters of the tilted grating-assisted null coupler.

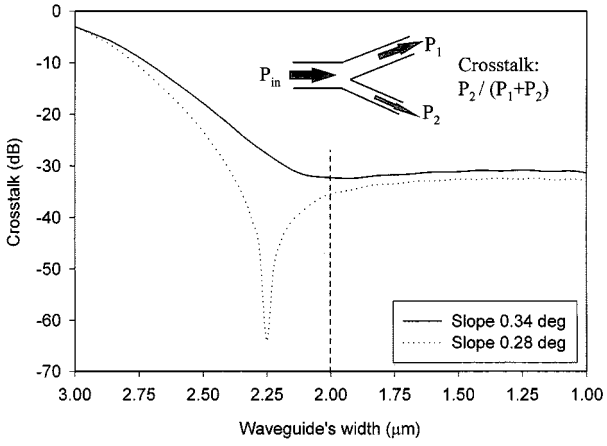

Fig. 4. Effect of the waveguide asymmetry to the crosstalk for two different slopes.

Authorized licensed use limited to: UNIVERSITY OF SOUTHAMPTON. Downloaded on October 7, 2009 at 07:15 from IEEE Xplore. Restrictions apply.

different slopes. The other waveguide has a fixed width of 3 μm. In both cases, the minimum and maximum waveguide separation is 0 μm (at the point where they touch to form the waist) and 15 μm (at the input end), respectively, resulting in different branch lengths. As input to the Y-branch is assumed the fundamental even eigenmode of the waist waveguide. It is first shown that $d_2 = d_1 = 3\,\mu$m results in -3 dB crosstalk that implies standard symmetric splitter. However, as the waveguide asymmetry increases, the crosstalk becomes progressively smaller which implies lack of efficient cross coupling (null coupler). It is shown that in order to obtain a crosstalk lower than about -30 dB, the waveguide width d_2 should be smaller than 2 μm, which corresponds to a V-number asymmetry ratio (V_2/V_1) smaller than about 0.67. However, it should be stressed that V_2 should be kept greater than 1.5 to minimize bending losses. It is also shown that, in general, a smaller branch slope results in lower crosstalk. For a slope of 0.28° and $d_2 = 2.252\,\mu$m, we observe a sharp decrease in crosstalk. This is a wavelength-sensitive resonant effect and should be avoided if we are interested in broadband operation.

Finally, the waveguide asymmetry and maximum separation (at the input/output ends) determines also the efficient excitation of the null coupler. To ensure single mode excitation at the input end, the ratio $\Delta\beta_{12}/C_{12}$ should be quite large [23]. $\Delta\beta_{12}(=\beta_1-\beta_2)$ is the difference of the propagation constants of the isolated waveguides (proportional to waveguide asymmetry) and C_{12} is the coupling constant between the two waveguide branches at the input end (inversely proportional to their separation). We have made sure that the asymmetries and maximum waveguide separations used in our designs always result in efficient single mode initial excitation at the input.

C. Taper Shape Optimization

In addition to waveguide asymmetry, power crosstalk is also determined by the shape of the coupler taper [24]. The shape optimization can be accomplished with a number of different methods, such as Genetic evolution strategies combined with beam propagation methods [25] and variational optimization techniques [26].

The variational optimization technique is easily implemented, fast converging and is adopted for optimising the null-coupler taper shape. In addition, it results in smoothly varying shapes that can be easily realized by modern, flexible UV-writing techniques [27]. For a certain crosstalk level, complex optimized shapes, on the other hand, can potentially result in overall shorter devices. For our purposes, we consider a generalized S-shape taper region, given by

$$S(z) = c_0 + \sum_{i=1}^{N-1} c_i \cos\left(i\frac{\pi}{L}z\right) \tag{2}$$

where L is the taper length. The N coefficients $c_i\,(i=0,\,N-1)$ form the weighting parameters of the optimization problem [26] which here targets to the reduction of the crosstalk to a fixed level. We have found that seven coefficients are enough to satisfactorily describe the taper region. Starting with an initial set of coefficients the optimization process adjusts them dynamically and is completed when a target crosstalk performance has been achieved. In this case, the target crosstalk was set at -55 dB with the even eigenmode initially excited. Full convergence was achieved after about 300 iterations. The initial and final S-shape coefficients c_i $(i = 0, 6)$ are $(7.497, -7.502, 10^{-3}, 10^{-3}, 10^{-3}, 10^{-3}, 10^{-3})$ and $(7.6197, -7.3788, -3.9345 \times 10^{-4}, -5.1494 \times 10^{-2}, 5.2274 \times 10^{-2}, -6.9656 \times 10^{-2}, -6.6957 \times 10^{-2})$, respectively. The same crosstalk level was achieved over a bandwidth of $\sim$40 nm, centered at 1550 nm. Fig. 5(a) shows the initial and final (optimized) taper shapes. This smooth optimized taper is described by a function which is free from discontinuities in the first and second derivatives, a characteristic which is quite important since any discontinuities of this kind can lead to increased bend transmission loss [28]. The inset shows the difference in local slopes between the two shapes. We can notice that the optimized taper shape exhibits higher local slopes at the initial part of the branch, which is in agreement with the general characteristics of shaped digital optical switches [24], [25]. Fig. 5(b) shows the evolution of the two normal eigenmodes (their normalized amplitudes) along

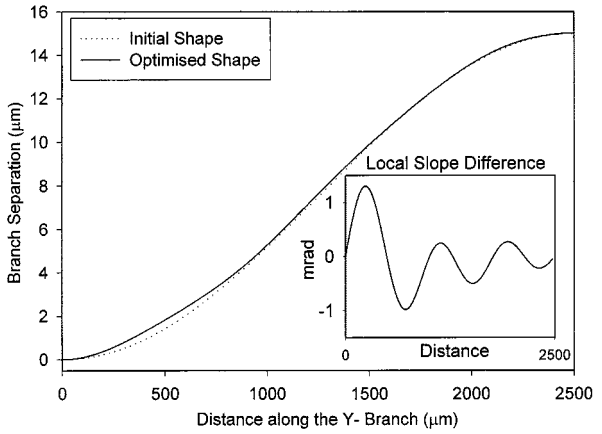

(a)

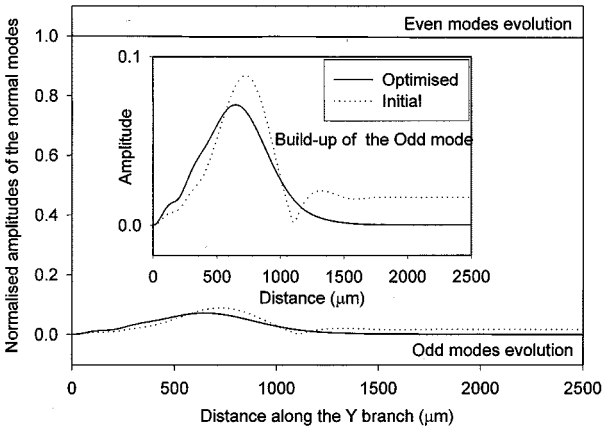

(b)

Fig. 5. (a) Optimized separation function for the Y branch and local slope difference (inset). (b) Comparison of mode evolution for the initial and the optimized null coupler.

Authorized licensed use limited to: UNIVERSITY OF SOUTHAMPTON. Downloaded on October 7, 2009 at 07:15 from IEEE Xplore. Restrictions apply.

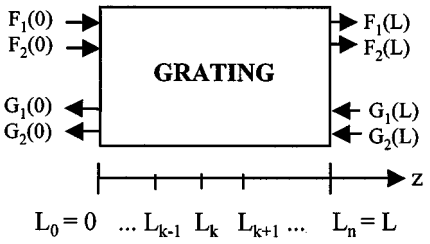

Fig. 6. Model for the calculation of the grating response.

the branch—when the even eigenmode at the waist was initially excited—for the initial (unoptimized) and final (optimized) taper shapes. The inset zooms into the amplitude evolution of the odd mode along the Y-branch. In the unoptimized case, the odd-mode build up shows a complex pattern that finally results in a residual excitation of the unwanted mode. The corrected local slopes of the optimized shape, on the other hand, counteract the initial build up and result in the target crosstalk.

IV. Analysis of the Grating Section

In this section, we concentrate on the analysis of the grating section in the coupler waist and consider the effect of the grating tilt on the total response. The theory is based on an original treatment by Weber [29] and takes into account the interaction between the forward- and backward-propagating coupler-waist eigenmodes. In our paper, the theory is further extended, through a transfer matrix approach, to cover nonuniform apodised gratings.

A. Spectral Response of a Nonuniform Grating

In the grating region, the amplitudes of the forward- and backward-propagating eigenmodes are denoted by $F_i(z)$ and $G_i(z)$, respectively, and $i = 1$ and 2 correspond to even and odd modes, respectively. The various quantities are shown schematically in Fig. 6. The total electric field in the grating region can be expressed as

$$E_g = \left\{ \left(F_1(z)e^{-j\beta_{g1}z} + G_1(z)e^{+j\beta_{g1}z}\right) \cdot \Psi_{\beta_{g1}}(x) + \left(F_2(z)e^{-j\beta_{g2}z} + G_2(z)e^{+j\beta_{g2}z}\right) \cdot \Psi_{\beta_{g2}}(x) \right\} e^{j\omega t} \tag{3}$$

where $\Psi_{\beta_{gi}}$ are the transverse field distributions and β_{gi} $(i = 1, 2)$ are the propagation constants of the ortho-normal eigenmodes at the coupler waist. The perturbation in the relative dielectric permittivity can be expressed, in terms of its spatial harmonics, as

$$\Delta\varepsilon_r(x, z) = \sum_{m\neq 0} \Delta\varepsilon_m(x) \cdot e^{-jm2(\pi/\Lambda)z} \tag{4}$$

where Λ is the period of the perturbation. In our analysis, we only retain the fundamental harmonic $(m = 1)$. The amplitude evolution is given by the following set of differential equations [29]:

$$\begin{aligned}
\frac{dF_1}{dz} &= -j\kappa_{11}G_1(z)e^{j2\Delta\beta_1 z} - j\kappa_{12}G_2(z)e^{j(\Delta\beta_1+\Delta\beta_2)z} \\
\frac{dF_2}{dz} &= -j\kappa_{12}G_1(z)e^{j(\Delta\beta_1+\Delta\beta_2)z} - j\kappa_{22}G_2(z)e^{j2\Delta\beta_2 z} \\
\frac{dG_1}{dz} &= j\kappa_{11}^*F_1(z)e^{-j2\Delta\beta_1 z} + j\kappa_{12}^*F_2(z)e^{-j(\Delta\beta_1+\Delta\beta_2)z} \\
\frac{dG_2}{dz} &= j\kappa_{12}^*F_1(z)e^{-j(\Delta\beta_1+\Delta\beta_2)z} + j\kappa_{22}^*F_2(z)e^{-j2\Delta\beta_2 z}
\end{aligned} \tag{5}$$

where $\Delta\beta_i = \beta_{gi} - K_B = \beta_{gi} - \pi/\Lambda$ $(i = 1, 2)$ is the phase detuning from the Bragg condition, and

$$\begin{aligned}
\kappa_{11} &= \frac{\omega\varepsilon_0}{4}\int_a^b \Delta\varepsilon_{+1}(x)\cdot\Psi_{\beta_{g1}}^2(x)\,dx \\
\kappa_{12} &= \kappa_{21}^* = \frac{\omega\varepsilon_0}{4}\int_a^b \Delta\varepsilon_{+1}(x)\cdot\Psi_{\beta_{g1}}(x)\cdot\Psi_{\beta_{g2}}(x)\,dx \\
\kappa_{22} &= \frac{\omega\varepsilon_0}{4}\int_a^b \Delta\varepsilon_{+1}(x)\cdot\Psi_{\beta_{g2}}^2(x)\,dx
\end{aligned} \tag{6}$$

are the three coupling coefficients governing the even–even (e–e), even–odd (e–o), and odd–odd (o–o) eigenmode interactions, respectively. The integration bounds a, b define the spatial transverse extension of the grating. By simple inspection of (5), it is obvious that there are *three* spectral regions of resonant power exchange between the even and odd waist eigenmodes. They are given by the relations $\Delta\beta_1 = 0$, $\Delta\beta_{12} = \Delta\beta_1 + \Delta\beta_2 = 0$, and $\Delta\beta_2 = 0$ and correspond to e–e, e–o, and o–o mode interactions, respectively. The relative strength of the interactions depends on the values of the relevant coupling coefficients and the amount of mode excitation at the null-coupler waist.

For a uniform grating of length $\Delta L = L_b - L_a$, (5) can be integrated to obtain the output fields in terms of the input counterparts, namely

$$\begin{pmatrix} F(L_b) \\ G(L_b) \end{pmatrix} = P(L_a, L_b)\begin{pmatrix} F(L_a) \\ G(L_a) \end{pmatrix} \tag{7}$$

where $F(z) = [F_1(z), F_2(z)]^T$, $G(z) = [G_1(z), G_2(z)]^T$, and $P(L_a, L_b)$ is the transfer matrix given by [29]

$$P(L_a, L_b) = \exp(S_1\Delta L)\exp(S_2\Delta L) \tag{8}$$

where

$$S_1 = \begin{pmatrix} j\Delta\beta_1 & 0 & 0 & 0 \\ 0 & j\Delta\beta_2 & 0 & 0 \\ 0 & 0 & -j\Delta\beta_1 & 0 \\ 0 & 0 & 0 & -j\Delta\beta_2 \end{pmatrix} \tag{9}$$

and (10), shown at the bottom of the next page. The exponential of the matrix S_2 can be, in general, calculated by means of the equivalent third degree polynomial [29].

Nonuniform apodised grating can be analyzed by dividing the structure into many uniform segments and applying (7)–(10)

Authorized licensed use limited to: UNIVERSITY OF SOUTHAMPTON. Downloaded on October 7, 2009 at 07:15 from IEEE Xplore. Restrictions apply.

iteratively following the transfer matrix method [30]. The total response of the nonuniform grating is then given by

$$\begin{pmatrix} F(L) \\ G(L) \end{pmatrix} = P_{\text{total}}(0, L) \cdot \begin{pmatrix} F(0) \\ G(0) \end{pmatrix} \tag{11}$$

where

$$\begin{aligned} P_{\text{total}}(0, L) = & P(L_{n-1}, L_n) \cdot P(L_{n-2}, L_{n-1}) \\ & \cdot \cdots \cdot P(L_1, L_2) \cdot P(L_0, L_1). \end{aligned} \tag{12}$$

The overall transfer matrix can be written in the form

$$P_{\text{total}}(0, L) = \begin{pmatrix} (P_{FF})_{2\times 2} & (P_{FG})_{2\times 2} \\ (P_{GF})_{2\times 2} & (P_{GG})_{2\times 2} \end{pmatrix}. \tag{13}$$

In the more general case, we need to estimate the normal modes $F(L)$ and $G(0)$ (which are the output modes on either side of the grating) as a function of the input normal modes $F(0)$ and $G(L)$. Equation (11) can then be easily transformed into the more useful form shown in (14) at the bottom of the page. Equation (14) determines the phase and amplitude of the reflected and transmitted normal modes at the grating section of the OADM.

B. Estimation of the Coupling Coefficients for a Tilted Grating

Next, we derive the basic expression of a tilted grating which will be used later to estimate the coupling coefficients and consequently the spectrum of the OADM. For $\theta = 0$, we have the special case of a phase grating written normal to the waveguide axis. The refractive index variation of the grating in Fig. 7 is expressed in the Cartecian system (X', Z') by the function

$$\Delta n(x', z') = \Delta n_0 \cdot \cos\left(\frac{2\pi}{\Lambda_g} z'\right). \tag{15}$$

By using the transformation $z' = x \sin\vartheta + z \cos\vartheta$ between the two Cartecian systems, it can be easily shown that the fundamental spatial harmonic of the relative dielectric permittivity perturbation [(4)], in the (X, Z) system, can be expressed as [29]:

$$\Delta\varepsilon_r(x, z) = (\Delta\varepsilon_{+1})_{\text{tilted}} \cdot e^{-j(2\pi/\Lambda)z} \tag{16}$$

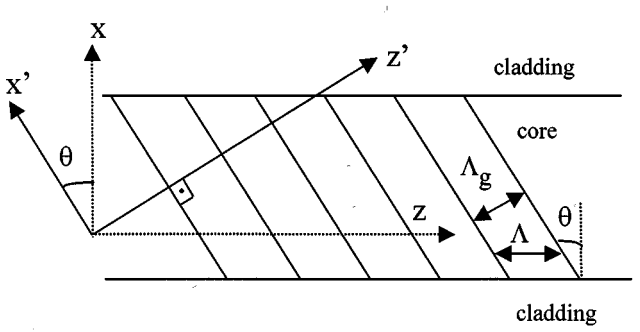

Fig. 7. Schematic of the tilted phase grating.

where $(\Delta\varepsilon_{+1})_{\text{tilted}} = \Delta\varepsilon_{+1} \cdot e^{-j((2\pi/\Lambda)\tan\vartheta)\cdot x}$, $\Delta\varepsilon_{+1} = \varepsilon_o \cdot \Delta n^2$, and $\Lambda = \Lambda_g/\cos\theta$. The coefficient $(\Delta\varepsilon_{+1})_{\text{tilted}}$ can be used in (6) to calculate the coupling coefficients of the tilted grating. In the case of an apodised grating, characterized along z' by a slowly varying apodization function $f(z')$, then along the waveguide axis (z-direction) the apodization profile is given by the projection of the original function along z-axis [30]. In the following analysis, the quoted apodization profiles are considered along the waveguide axis z (or z'), given that modern UV-writing techniques [31] enable the writing of the desired complex profiles along z.

C. Tilted Grating Optimization

The operation of the proposed OADM is based on the grating-assisted, efficient cross coupling between the even and odd eigenmodes (e–o interaction) at the coupler waist. This resonant power transfer takes place at a wavelength λ_o here the $\beta_e(\lambda_o) + \beta_o(\lambda_o) = 2\pi/\Lambda$ Bragg condition is satisfied. As already mentioned in Section IV-A, in addition to λ_o, there are two extra wavelengths λ_1 and λ_2 where even–even (e–e) and odd–odd (o–o) mode interactions take place. The wavelengthsλ_1 and λ_2 fulfill the Bragg conditions $\beta_e(\lambda_1) = \pi/\Lambda$ and $\beta_o(\lambda_2) = \pi/\Lambda$ respectively with $\lambda_1 > \lambda_o > \lambda_2$. In the general case, the e–e and o–o interactions result in two extra reflection peaks, centered at λ_1 and λ_2, respectively. These two unwanted peaks can potentially

$$S_2 = \begin{pmatrix} -j\Delta\beta_1 & 0 & -j\kappa_{11}e^{j2\Delta\beta_1 z} & -j\kappa_{12}e^{j(\Delta\beta_1+\Delta\beta_2)z} \\ 0 & -j\Delta\beta_2 & -j\kappa_{12}e^{j(\Delta\beta_1+\Delta\beta_2)z} & -j\kappa_{22}e^{j2\Delta\beta_2 z} \\ j\kappa_{11}^* e^{-j2\Delta\beta_1 z} & j\kappa_{12}^* e^{-j(\Delta\beta_1+\Delta\beta_2)z} & j\Delta\beta_1 & 0 \\ j\kappa_{12}^* e^{-j(\Delta\beta_1+\Delta\beta_2)z} & j\kappa_{22}^* e^{-j2\Delta\beta_2 z} & 0 & j\Delta\beta_2 \end{pmatrix}_{z=L_a}. \tag{10}$$

$$\begin{pmatrix} F_1(L) \\ F_2(L) \\ G_1(0) \\ G_2(0) \end{pmatrix}_{4\times 1} = \begin{pmatrix} (P_{FF} - P_{FG} \cdot P_{GG}^{-1} \cdot P_{GF})_{2\times 2} & (P_{FG} \cdot P_{GG}^{-1})_{2\times 2} \\ -(P_{GG}^{-1} \cdot P_{GF})_{2\times 2} & (P_{GG}^{-1})_{2\times 2} \end{pmatrix}_{4\times 4} \cdot \begin{pmatrix} F_1(0) \\ F_2(0) \\ G_1(L) \\ G_2(L) \end{pmatrix}_{4\times 1}. \tag{14}$$

Authorized licensed use limited to: UNIVERSITY OF SOUTHAMPTON. Downloaded on October 7, 2009 at 07:15 from IEEE Xplore. Restrictions apply.

interfere with other optical channels and severely impair the OADM performance. Their strength depends on the degree of even and odd mode excitation at the waist and the strength of the corresponding coupling constant [see (6)]. Strong e–e and o–o interactions would result in significant backreflections at the high and low V-number input waveguides, respectively. In addition to branch-asymmetry and taper-shape optimizations, the grating tilt angle and grating extend can be also properly chosen to eliminate the unwanted reflection peaks.

The three coupling coefficients κ_{eo}, κ_{ee} and κ_{oo} of a tilted grating, given by (6) and (16), are plotted in Fig. 8(a)–(c) as a function of the tilt angle, for different coupler geometries and grating extends. In Fig. 8(a) and 8(b), on the other hand, the two waveguides are in full contact along the waist. In Fig. 8(c) ,the two dissimilar waveguides are separated by 1 μm along the null-coupler waist. In Fig. 8(a) and 8(c), the grating is written in the core areas only (only the cores are assumed photo-sensitive), while in Fig. 8(b) the grating is extended outside the core area (core and cladding are assumed equally photo-sensitive). The amplitude of the refractive-index modulation is assumed to be $\Delta n = 10^{-3}$.

It is shown that, in the cases a) and b), there is always an optimum tilt-angle (θ_0) where the e–o cross-coupling acquires a near-maximum value *and* the o–o self-coupling is zero. This implies that when $\theta = \theta_0$, launching light into port 2 (low V-number input) of the OADM will result in maximum cross-coupling, i.e., efficient drop action, without any self-coupling, i.e., backreflections. It should be also mentioned that, when $\theta = \theta_0$, launching light into port 3, results in equally efficient cross-coupling and add OADM function (at λ_0), as well as a sizeable e–e self-coupling and strong backreflection (although at a different wavelength λ_1) (see spectra in Fig. 14). This backreflection might necessitate the use of an isolator at this port. In case c), however, where the two photosensitive cores are separated, the tilt angle that corresponds to maximum e–o interaction *does not* result simultaneously in zero o–o self-coupling. Therefore, such OADM geometry will always suffer from strong backreflections at both drop and add input ports. It should be mentioned that this geometry is pertinent to a recently reported fiber-optic implementation of this OADM [15].

Tilted gratings, however, in addition to guided modes are known to excite cladding [32], as well as, leaky and radiation [33] modes. Although the coupling into these modes and the related losses are not covered in this paper, the effect of the various parameters on the optimum tilt angle is considered in some detail.

Fig. 9(a) shows the variation of the optimum tilt angle (θ_0) as a function of the normalized grating width (d_g/d_w) for three different widths (and different V-numbers). The refractive indices are same as in Fig. 3. Fig. 9(b), on the other hand, shows the corresponding variation of the actual coupling constants κ_{eo}, κ_{ee} ($\kappa_{oo} = 0$ since $\theta = \theta_0$ throughout). It is shown that extending the grating into the cladding reduces significantly θ_0. The degree of grating-extent, for this reduction to take place, increases for lower V-number waveguides because of the significant part of the mode-power spreading into the cladding. For extents larger than this minimum-required-extent (which depends on the V-number) the minimum θ_0 and κ_{eo}, κ_{ee} remain

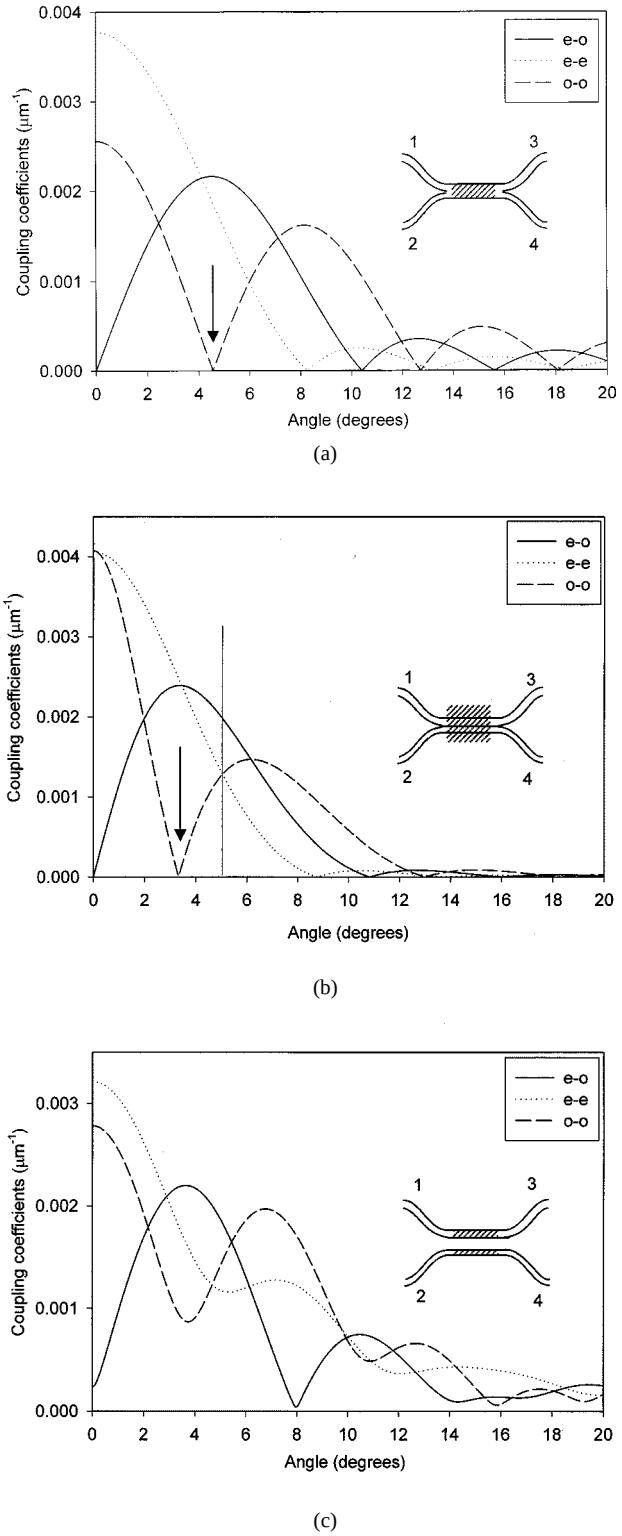

Fig. 8. (a) Coupling coefficients versus tilt angle when the grating is inscripted only at the single-core waist (waveguide's separation: $h = 0$ μm). (b) Coupling coefficients versus tilt angle when the grating is extended deeply into the equally photosensitive cladding region. (c) Coupling coefficients versus tilt angle when the asymmetric waveguides at the waist of the coupler are separated by a distance: $h = 1$ μm.

constant. This is because beyond this value both eigenmodes overlap fully with the grating. For gratings restricted inside the core area $(d_g/d_w < 1)$, θ_0 is shown to increase sharply while κ_{eo} and κ_{ee} decrease significantly. Combinations of small θ_0

Authorized licensed use limited to: UNIVERSITY OF SOUTHAMPTON. Downloaded on October 7, 2009 at 07:15 from IEEE Xplore. Restrictions apply.

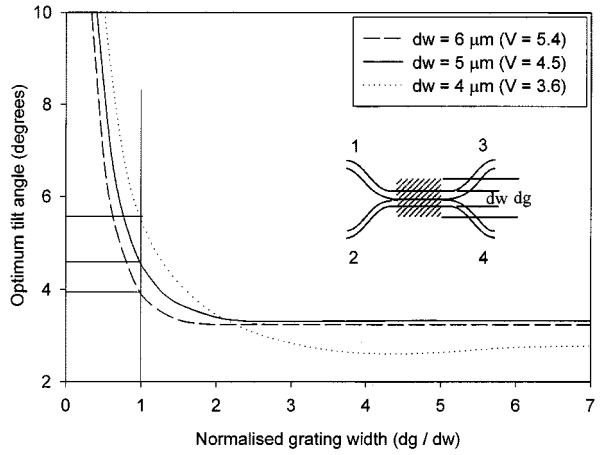

(a)

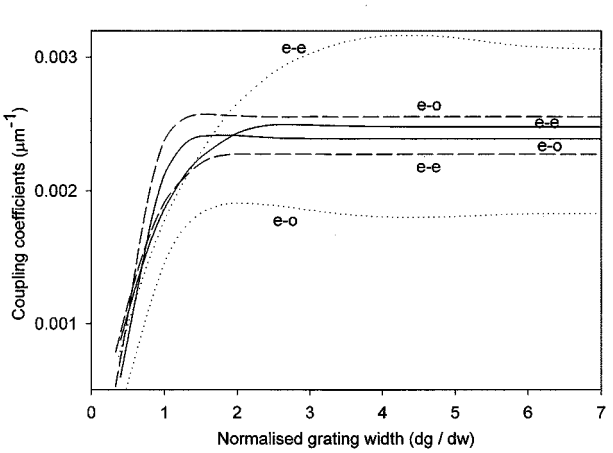

(b)

Fig. 9. (a) Relation between the optimum tilt angle and the grating's extent for coupler waists with different V-numbers. (b) Coupling coefficient at the optimum operational point, as a function of grating's extent.

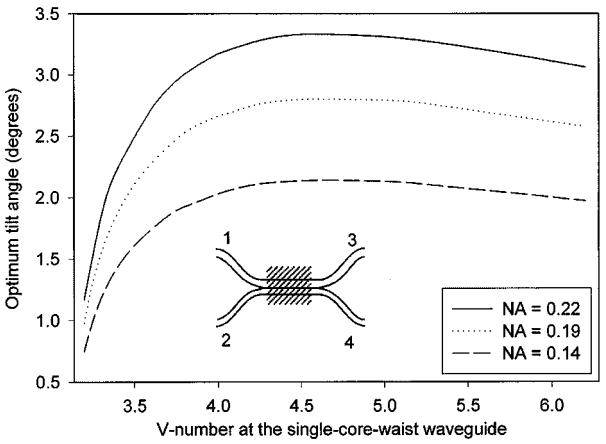

(a)

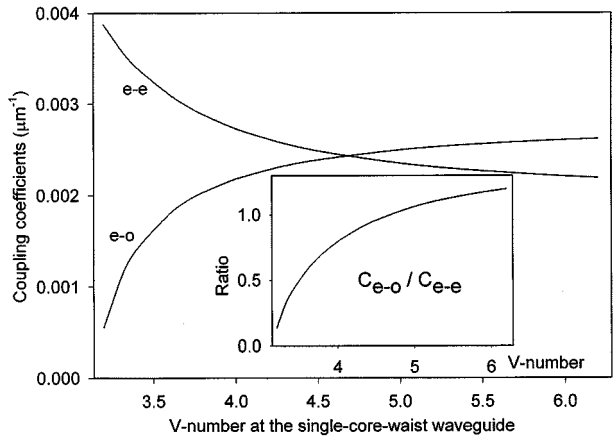

(b)

Fig. 10. (a) Effect of the V-number to the optimum tilt angle for waveguides with different NAs. (b) Effect of the V-number to the coupling coefficients at the optimum-operational point for waveguides with different NAs.

and large κ_{eo} are obviously required in order to achieve (for a given length) strong gratings with negligible radiation losses.

For the case of a single-core waist in step-index geometry, considered here, we can derive analytical expressions, which relate the optimum tilt angle to the waist parameters. These relations are given in the Appendix for the gratings restricted in the core only or extended into the infinite cladding. Fig. 10(a) and (b) shows the variation of the optimum tilt angle (θ_0) and coupling coefficients $(\kappa_{eo}, \kappa_{ee})$, respectively, as a function of the single-core waist V-number, for different numerical apertures (NAs). The grating is extended infinitely into the cladding. The V-number range is restricted to $\pi \leq V \leq 2\pi$ so that the waist supports only the two lowest-order eigenmodes. It is shown that, for a fixed waist V-number, the lower the NA, the smaller the optimum tilt angle. This is due to the fact that lower NAs result in lower mode confinement and, therefore, smaller θ_0. For V-numbers just above π, the odd mode is close to cutoff and extends deep into the cladding. As a result the optimum tilt angles, at this point, reduce sharply toward zero. For all NAs, the optimum tilt angle acquires a maximum at $V \cong 4.5$. The coupling coefficients κ_{eo} (κ_{ee}) increase (decrease) monotonically with waist V-number. Due to complete grating/mode(s) overlap, on the other hand, both coupling coefficients are independent of the waist NA, so the e–o and e–e coupling coefficients for the three different NAs correspond to the two single curves in Fig. 10(b). The inset in Fig. 10(b) finally gives the ratio of the coupling coefficients κ_{eo}, κ_{ee}. From Fig. 10, it is deduced that low-NA, high V-number waists should be favored in order to obtain strong gratings with minimum tilt angle. However, the low-NA choice should be compromised in order to minimize bending losses at the coupler taper region.

Throughout the analysis, we have assumed that core and cladding material have the same photosensitivity and acquire the same refractive-index modulation. This is possible by proper choice of the core and cladding codoping materials and the UV-writing wavelength. We have also considered the more general case where the core and cladding regions acquire different peak index modulation. In this case, the obtained optimum tilt angles are slightly smaller than and follow the same trends with the ones shown in Figs. 9 and 10.

Authorized licensed use limited to: UNIVERSITY OF SOUTHAMPTON. Downloaded on October 7, 2009 at 07:15 from IEEE Xplore. Restrictions apply.

V. Full Spectral Response of the OADM

In Sections III and IV, we considered the various null-coupler and tilted-grating optimization steps, respectively, and discussed design criteria for the waveguide asymmetry the taper shape and the grating tilt and extend. In this section, we take into account the aforementioned findings and combine the theories presented in Sections III-A and IV-A in order to obtain the full spectral response of various OADM configurations.

The fundamental mode of the individual input-port waveguide is excited and then propagated along the structure determining this way the amplitudes and phases of the two normal modes before they enter the grating. At the waist region, where the grating is written, we calculate the forward and backward propagating modes and continue propagating them along the coupler to all the ports of the device. In this way, for light launched into input port (2), we calculate the full spectra at the drop port (1), the backreflected light (at the input port), the transmitted light (at port 4) and the cross-coupled light at the add port (3).

In the following analysis, we assume that the individual waveguide widths are $d_1 = 3\ \mu$m, $d_2 = 2\ \mu$m, and the coupler waist width is $d_w(= d_1 + d_2) = 5\ \mu$m. The core/cladding refractive indices are the same with the ones in Fig. 1. The grating is extended deeply into the cladding and the corresponding optimum tilt angle is 3.33°. The grating length is considered to be 4 mm and the amplitude of the refractive index modulation is 10^{-3}. A raised cosine apodization profile is assumed. The period of the grating is adjusted for the different tilt angles in order to optimize always the Drop and Add operations at 1550 nm.

A. Linear-Branch Coupler—Nonoptimum Grating Tilt

We first demonstrate the effect of partial optimization on the OADM performance by considering null couplers with linear branches. As already discussed in Section IV-B, such a coupler design results in relatively high crosstalk for most of the waveguide branch asymmetries (see Fig. 4). The branch slope is 0.28° and the corresponding crosstalk is about −30 dB. The lower V-number port 2 is used as the OADM input port. Since $V_2 < V_1$, the input light excites predominantly the odd eigenmode in the waist region. The even-mode power in the same region is ∼−30 dB below the odd-mode one.

In Fig. 11(a) and (b), the calculated spectra at the drop port (1) and output port (4) are shown, along with the backreflected spectra at the input port (2) and the crosstalk spectrum at port 3. In this case, the grating tilt angle is 5° (nonoptimum) and the corresponding coupling coefficients are $\kappa_{ee} = \kappa_{oo} = 0.0012\ \mu\text{m}^{-1}$, and $\kappa_{eo} = \kappa_{oe} = 0.002\ \mu\text{m}^{-1}$ [see Fig. 8(b)]. In Fig. 11(a), three distinct regions (A, B, and C) can be seen centered around 1545 nm, 1550 nm, and 1555 nm, respectively. The various peaks in the drop (solid line) and backreflected (dashed line) spectra have different physical origin and involve different coupling mechanisms. First, it should be reminded that the solid- and dashed-line responses involve the excitation backward-propagating even and odd eigenmode, respectively, at the coupler waist. Second, the three aforementioned regions correspond to odd–even (A), odd–odd (B), and even–even (C) resonant grating-assisted (Bragg) power exchange.

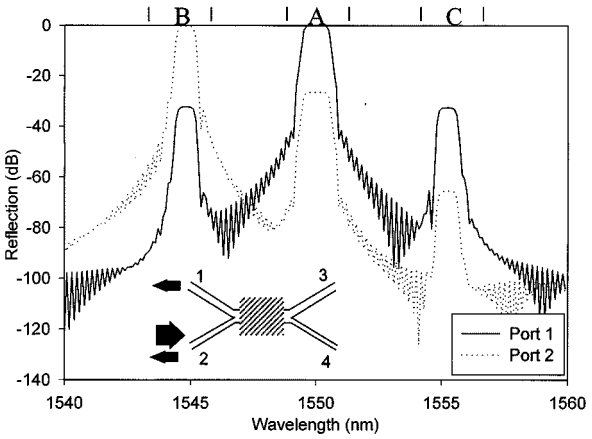

(a)

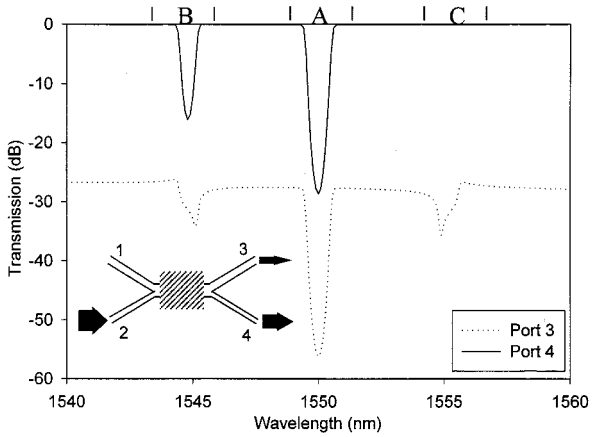

(b)

Fig. 11. Spectral response of the OADM with linear coupler and grating with nonoptimum tilt angle (Drop action): (a) reflection spectra and (b) transmission spectra.

1) Region A: The solid-line peak, in region A, corresponds to resonant odd–even mode power transfer (determined by κ_{oe}) and constitutes the main feature in the drop action. The dashed-line peak, in the same region, corresponds to the power transfer by two different mechanisms: First, because of the resonant power transfer between the residual even mode (−30 dB below the dominant odd mode) to the odd mode, which is determined by κ_{eo}. Second, partial excitation of the odd mode during the backward-propagation of the even mode to port 1 along the taper region.

2) Region B: The dashed-line peak, in region B, corresponds to odd–odd mode resonant (Bragg) backreflection (determined by κ_{oo}). The solid-line peak, in the same region, is due to the fact that the backward-propagating odd mode excites partially the even mode during its propagation along the taper region. Since in this coupler design the taper-induced crosstalk is −30 dB, the solid-line peak B is a replica of the dashed-line peak B, downshifted by this amount.

3) Region C: Finally, the solid-line peak, in region C, corresponds to the residual even–even mode resonant (Bragg) backreflection (determined by κ_{ee}). The dashed-line peak, in the same region, is due to the fact that the backward-propagating even

Authorized licensed use limited to: UNIVERSITY OF SOUTHAMPTON. Downloaded on October 7, 2009 at 07:15 from IEEE Xplore. Restrictions apply.

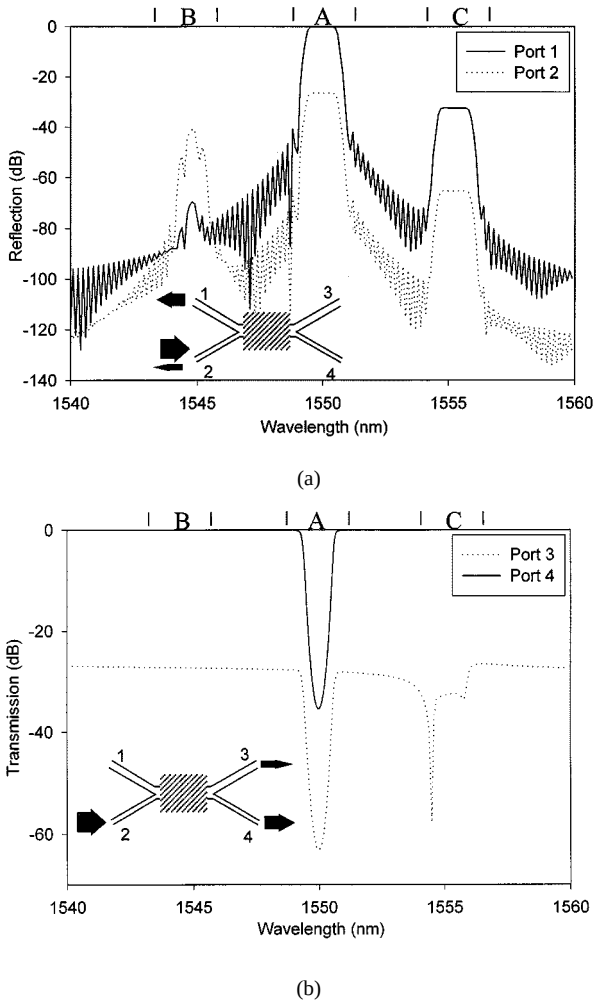

Fig. 12. Spectral response of the OADM with linear coupler and grating with optimimum tilt angle (Drop action): (a) reflection spectra and (b) transmission spectra.

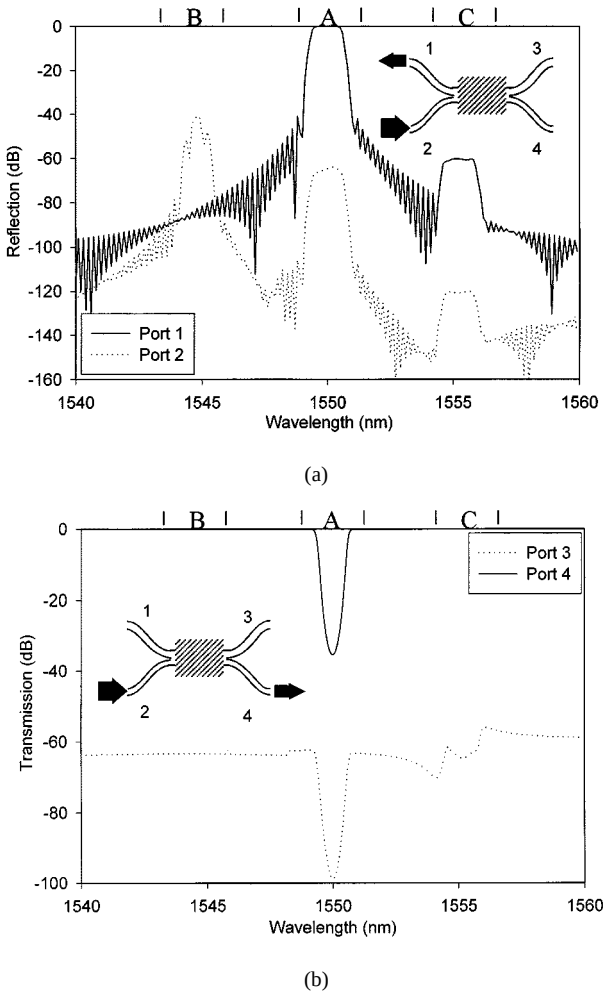

Fig. 13. Spectral response of the OADM with optimized null coupler and optimimum tilt angle (Drop action): (a) reflection spectra and (b) transmission spectra.

mode now excites partially the odd mode during its propagation along the taper region. Again, since the taper- induced crosstalk is -30 dB for this design, the dashed-line peak C is a replica of the solid-line peak C, downshifted by the same amount.

Fig. 11(b) shows the transmitted (solid line) and cross-coupling (dashed line) spectra. The two notches in the transmission spectrum correspond to the odd–even and odd–odd resonant backreflections shown in Fig. 11(a). Since $\kappa_{oe} > \kappa_{oo}$, the notch in region A is deeper than the one in region B. The cross-coupled power is determined by the taper shape. Although the Y-branches used here for the construction of the coupler, exhibit crosstalk level better than -30 dB the resulted crosstalk level for the coupler is ~ -27 dB. That can be explained by taking into consideration the additional partial residual excitation of the even mode at the first half part of the coupler where the low V-number waveguide was excited.

B. Linear-Branch Coupler—Optimum Grating Tilt

Next, we consider the effect of the optimum grating tilt on the OADM performance. The tilt angle is $\sim 3.33°$, while the coupler configuration and the rest of the parameters are the same as in the previous case A. From Fig. 8(b), it is deduced that in this case the odd–odd coupling coefficient diminishes ($\kappa_{oo} \cong 0$), while both odd–even and even–even coefficients increase ($\kappa_{oe} \cong \kappa_{ee} \cong 0.0024\ \mu\text{m}^{-1}$), in comparison with the previous case.

The most obvious spectral change is observed in region B, where, due to the diminished κ_{oo} coefficient, the dashed-line peak is reduced below -40 dB. At the same time, the corresponding transmission notch disappears. All the other features in spectral regions A and C (determined by κ_{oe}, κ_{ee} and the taper-induced cross-coupling) remain unchanged. Actually due to increased κ_{oe} and κ_{ee}, the grating strength is increased. This is shown by the increase in both the 3-dB bandwidth at the drop port [Fig. 12(a)] and the depth of the transmission notch [Fig. 12(b)]. The OADM crosstalk [dashed line in Fig. 12(b)], on the other hand, remains at the same level as in Fig. 11(b), since the coupler design remains unchanged.

C. Fully Optimized Null-Coupler OADM—Drop Operation

We now turn our attention to the performance of fully optimized OADMs. We employ a S-shape taper region optimized to give -55 dB of crosstalk (see Section III-C). The optimum tilt

Authorized licensed use limited to: UNIVERSITY OF SOUTHAMPTON. Downloaded on October 7, 2009 at 07:15 from IEEE Xplore. Restrictions apply.

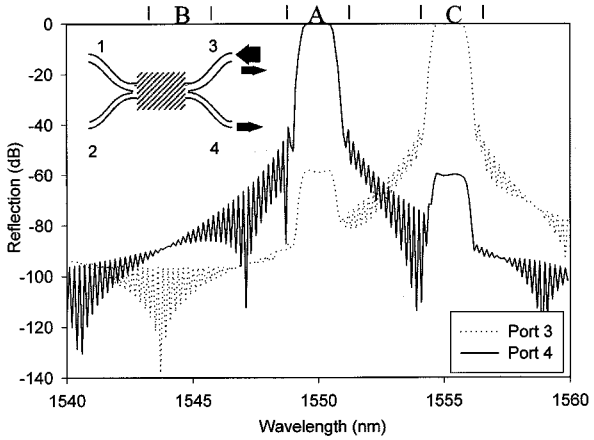

(a)

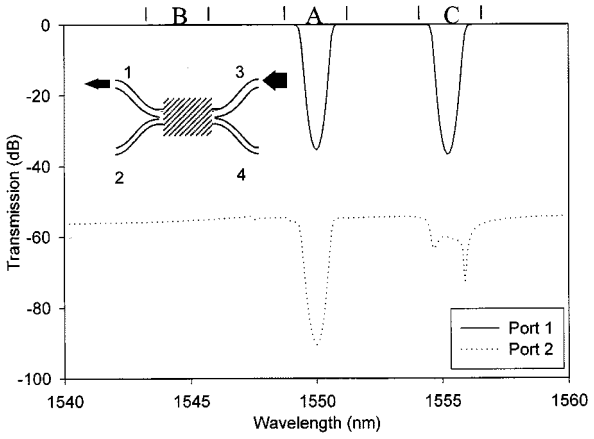

(b)

Fig. 14. Spectral response of the OADM with optimized null coupler and optimimum tilt angle (Add action): (a) reflection spectra and (b) transmission spectra.

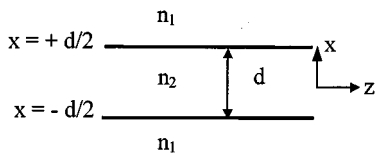

Fig. 15. Schematic of a three-layer symmetric waveguide.

angle and the rest of the waveguide and grating parameters are the same as in the previous case B.

Fig. 13(a) shows the full drop (solid line) and backreflected (dashed line) OADM spectra. Fig. 13(b) shows the corresponding transmitted (solid line) and cross-coupled (dashed line) spectra. Compared with the response in Fig. 12, the solid-line drop peak in region A and the dashed-line backreflected peak in region B are unchanged, since they depend solely on κ_{oe} and κ_{ee}, respectively, which in turn depend on the grating tilt angle and extent. The remaining three peaks in Fig. 13(a) depend predominantly on the taper-induced crosstalk and are reduced to a level below -55 dB. Similar effects are observed in Fig. 13(b).

Fig. 13(a) and (b) shows that a fully optimized null-coupler-based OADM provides a single well-defined peak in drop spectrum accompanied by a single notch in the corresponding transmission spectrum. All the other features, originating from the grating and taper-induced crosstalk, remain well below a level that is set by the optimized taper shape and grating tilt.

D. Fully Optimized Null-Coupler OADM—Add Operation

Finally, we consider the spectral response of the fully optimized OADM, considered in Section V-C, under add-mode operation. In this case, light is launched into port 3 and is expected to appear in the transmission port 4. Fig. 14(a) shows the full add (port 4-solid line) and backreflected (port 3-dashed line) spectra. It is shown that due to reciprocity, the "add" spectrum is identical with the drop spectrum [see Fig. 13(a)]. The backreflected spectrum, however, shows a very strong peak (dashed line in region C) due to the large κ_{ee}. Actually, since $\kappa_{ee} \cong \kappa_{eo}$ in the present case, the add and backreflected peaks are similar. This is further manifested by the similar size notches in the corresponding transmission spectrum shown in Fig. 14(b) (solid line). The strong backreflection at the "add" port 3 is *out of the "add" band* and can be further reduced by increasing the waist V-number [see Fig. 10(b)]. Otherwise, the effect can be totally suppressed by the insertion of one optical isolator.

The dashed line in Fig. 14(b) shows the cross-coupling into port 2, determined by the taper shape. Since in this case the high V-number waveguide (and consequently the even supermode of the structure) was initially excited the crosstalk level is in absolute agreement with the performance of the optimized S-bent branch which was designed by assuming excitation with the even waist mode. The different crosstalk level in Fig. 13(b) (which again is below -55 B) should be attributed to the fact that the coupler now is excited by the odd supermode.

VI. Conclusion

We have thoroughly studied the performance of fully optimized OADMs based on null couplers and tilted Bragg gratings. We have shown that maximization of the device performance involves three main optimization steps. First, the waveguide asymmetry (V_2/V_1 ratio) should be optimized in order to minimize the extinction ratio of the unwanted mode at the null coupler waist. Second, the coupler taper shape should be optimized in order to further minimize the aforementioned extinction ratio. Third, the grating tilt angle and relative width can be also optimized to give negligible backreflections at the input port and minimize radiation losses.

We have shown that keeping V_2/V_1 at $\sim$0.67 and employing an optimized S-bent coupler taper, the unwanted-mode extinction ratio at the coupler waist is kept at about -55 dB. Finally, a fully optimized OADM is shown to provide a drop action with crosstalk better than -40 dB. The backreflections at the input port are also kept below -40 dB. These results show that the proposed high-performance OADM configuration can meet the stringent telecom specifications. Since the relative width of

Authorized licensed use limited to: UNIVERSITY OF SOUTHAMPTON. Downloaded on October 7, 2009 at 07:15 from IEEE Xplore. Restrictions apply.

the grating is great importance, the device can be best-implemented in integrated optics form. FHD planar technology combined with UV waveguide- and grating-writing techniques can be well suited for a the practical device implementation.

It should be also stressed that, in contrast with other OADM configurations that involve gratings in the waist of SFCs [10] (discussed in the introduction), the performance of the present null-coupler OADM does not depend on the grating position. On the other hand, since the optimized device operation relies on grating-assisted coupling, the spectral and dispersion characteristics of the "drop" and "add" channels are replicas of the grating counterparts. In that respect, the OADM characteristics can be fully tailored by using recent advanced design algorithms [34].

APPENDIX
ANALYTICAL EXPRESSIONS FOR THE OPTIMUM TILT ANGLE

For the symmetrical three-layer configuration (Fig. 15) the transverse electric field for the odd TE-mode can be expressed as [35]

$$E_y(x) = \begin{cases} \sin\left(h\frac{d}{2}\right)\exp\left(-q\left(x-\frac{d}{2}\right)\right) & x \geq \frac{d}{2} \\ \sin(hx) & -\frac{d}{2} \leq x \leq \frac{d}{2} \\ -\sin\left(h\frac{d}{2}\right)\exp\left(+q\left(x+\frac{d}{2}\right)\right) & x \leq -\frac{d}{2} \end{cases}$$

where

q $= \sqrt{\beta^2 - n_1^2 k^2}$;
h $= \sqrt{n_2^2 k - \beta^2}$;
k $= \omega/c$;
β propagation constant obtained from the dispersion equation: $\cot(h(d/2)) = -(q/h)$.

When the grating is written in the core region only, the optimum tilt angle Θ where the zero o–o coupling occurs, is related with the other waveguide parameters by the expression:

$$\sin\left(C\frac{d}{2}\right)\{C^2[2(\cos(hd)-1)]+8h^2\} + \cos\left(C\frac{d}{2}\right)\{C[-4h(\sin(hd))]\} = 0$$

When the grating is extended into the infinite cladding the expression takes the form:

$$\sin\left(C\frac{d}{2}\right)\{C^2[8(q^2+h^2)\cos(hd)-8q^2]+32h^2q^2\} + \cos\left(C\frac{d}{2}\right)\{C[-16qh[h(\cos(hd)-1)+q\sin(hd)]] + C^3[4[q(\cos(hd)-1)-h\sin(hd)]]\} = 0$$

The parameter $C = (2\pi/\Lambda)\tan(\Theta)$ contains in both cases the optimum tilt angle Θ.

ACKNOWLEDGMENT

The authors would like to thank Dr. P.G.R. Smith and Dr. R. Feced for their valuable contributions to this work.

REFERENCES

[1] K. P. Jones, M. S. Chadry, D. Simeonidou, N. H. Taylor, and P. R. Morkel, "Optical wavelength add–drop multiplexer in installed submarine WDM network," *Electron. Lett.*, vol. 31, no. 24, pp. 2117–2118, Nov. 1995.
[2] D. C. Johnson, K. O. Hill, F. Bilodeau, and S. Faucher, "New design concept for a narrowband wavelength-selective optical tap and combiner," *Electron. Lett.*, vol. 23, pp. 668–669, 1987.
[3] T. Erdogan, T. A. Strasser, M. A. Milbrodt, E. J. Laskowski, C. H. Henry, and G. E. Kohnke, "Integrated-optical Mach-Zehnder add–drop filter fabricated by a single UV-induced grating exposure," *Appl. Opt.*, vol. 36, pp. 7838–7845, 1997.
[4] F. Bilodeau, K. O. Hill, B. Malo, D. C. Johnson, and J. Albert, "High-return-loss narrow-band all-fiber bandpass bragg transmission filter," *IEEE Photon. Technol. Lett.*, vol. 6, no. 1, pp. 80–82, Jan. 1994.
[5] R. Kashyap, G. D. Maxwell, and B. J. Ainslie, "Laser-trimmed four-port bandpass filter fabricated in single-mode photosensitive Ge-doped planar waveguide," *IEEE Photon. Technol. Lett.*, vol. 5, no. 2, pp. 191–194, Feb. 1993.
[6] F. Bilodeau, D. C. Johnson, S. Theriault, B. Malo, J. Albert, and K. O. Hill, "An all-fiber dense-wavelength-division multiplexer/demultiplexer using photoimprinted bragg gratings," *IEEE Photon. Technol. Lett.*, vol. 7, no. 4, pp. 388–390, Apr. 1995.
[7] J. Albert, F. Bilodeau, D. C. Johnson, K. O. Hill, K. Hattori, T. Kitagawa, Y. Hibino, and M. Abe, "Low-loss planar lightwave circuit OADM with high isolation and no polarization dependence," *IEEE Photon. Technol. Lett.*, vol. 11, no. 3, pp. 346–348, Mar. 1999.
[8] D. Marcuse, *Theory of Dielectric Optical Waveguides*. New York: Academic, 1991, ch. Ch. 7.
[9] J.-L. Archambault, P. S. J. Russell, S. Barcelos, P. Hua, and L. Reekie, "Grating frustrated coupler: A novel channel-dropping filter in single-mode optical fiber," *Opt. Lett.*, vol. 19, pp. 180–182, 1994.
[10] K. Bakhti, P. Sansonetti, C. Sinet, L. Gasca, L. Martineau, S. Lacroix, X. Daxhelet, and F. Gonthier, "Optical add–drop multiplexer based on UV written Bragg gratings in a fused 100% coupler," *Electron. Lett.*, vol. 33, no. 9, pp. 803–804, Apr. 1997.
[11] R. Kashyap, "A simplified approach to Bragg grating based Michelson and the in-coupler Bragg grating add–drop multiplexers," in *Proc. Optic. Fiber Commun. Conf. (OFC' 99)*, San Diego, CA, Feb. 21–26, 1999, paper TuN3.
[12] M. S. Whalen, M. D. Divino, and R. C. Alferness, "Demonstration of a narrowband Bragg-reflection filter in a single-mode fiber directional coupler," *Electron. Lett.*, vol. 22, no. 12, pp. 681–682, Jun. 1986.
[13] P. Yeh and H. F. Taylor, "Contradirectional frequency-selective couplers for guided wave optics," *Appl. Opt.*, vol. 19, no. 16, pp. 2848–2855, Aug. 1980.
[14] L. Dong, P. Hua, T. A. Birks, L. Reekie, and P. St. Russell, "Novel add–drop filters for wavelength-division multiplexing optical fiber systems using a Bragg grating assisted mismatched coupler," *IEEE Photon. Technol. Lett.*, vol. 8, no. 12, pp. 1656–1658, Dec. 1996.
[15] A. S. Kewitsch, G. A. Rakuljic, P. A. Willems, and A. Yariv, "All fiber zero insertion loss add drop filter for WDM," *Opt. Lett.*, vol. 23, no. 2, pp. 106–108, Jan. 1998.
[16] C. K. Madsen, T. A. Strasser, M. A. Milbrodt, C. H. Henry, A. J. Bruce, and J. DeMarco, "Planar waveguide add/drop filter employing a mode-converting grating in an adiabatic coupler," in *Proc. Integrated Photonics Research Conf.*, Victoria, Canada, 1998, paper IMG5, pp. 102–104.
[17] T. Erdogan, "Optical add–drop multiplexer based on asymmetric Bragg coupler," *Opt. Commun. 157*, pp. 249–264, Dec. 1998.
[18] T. A. Birks, S. G. Farwell, P. S. J. Russell, and C. N. Panell, "Four-port fiber frequency shifter with a null taper coupler," *Opt. Lett.*, vol. 19, no. 23, pp. 1964–1966, Dec. 1994.
[19] S. G. Farwell, M. N. Zervas, and R. I. Laming, "2 × 2 fused fiber null couplers with asymmetric waist cross sections for polarization independent (< 0.01 dB) switching," *J. Lightwave Technol.*, vol. 16, no. 9, pp. 1671–1679, Sept. 1998.

Authorized licensed use limited to: UNIVERSITY OF SOUTHAMPTON. Downloaded on October 7, 2009 at 07:15 from IEEE Xplore. Restrictions apply.

[20] C. Riziotis and M. N. Zervas, "Optimization of OADM's based on grating assisted mode conversion in null couplers," in *Proc. Eur. Conf. Optic. Communication (ECOC'99)*, Nice, France, Sept. 21–26, 1999, TuD1.6.
[21] W. K. Burns and A. F. Milton, "Mode conversion in planar-dielectric separating waveguides," *IEEE J. Quantum Electron.*, vol. QE-11, no. 1, pp. 32–39, Jan. 1975.
[22] H. Yajima, "Coupled mode analysis of dielectric planar branching waveguides," *IEEE J. Quantum Electron.*, vol. QE-14, no. 10, pp. 749–755, Oct. 1978.
[23] A. F. Milton and W. K. Burns, "Tapered velocity couplers for integrated optics: Design," *Appl. Opt.*, vol. 14, no. 5, pp. 1207–1212, May 1975.
[24] W. K. Burns, "Shaping the digital switch," *IEEE Photon. Technol. Lett.*, vol. 4, no. 8, pp. 861–863, Aug. 1992.
[25] R. Moosburger, C. Kostrzewa, G. Fischbeck, and K. Petermann, "Shaping the digital optical switch using evolution strategies and BPM," *IEEE Photon. Technol. Lett.*, vol. 9, no. 11, pp. 1484–1486, Nov. 1997.
[26] B. E. Little, "Filter synthesis for coupled waveguides," *J. Lightwave Technol.*, vol. 15, no. 7, pp. 1149–1155, Jul. 1997.
[27] M. Svalgaard, "Direct writing of planar waveguide power splitters and directional couplers using a focused ultraviolet laser beam," *Electron. Lett.*, vol. 33, no. 20, pp. 1694–1695, Sept. 1997.
[28] W. J. Minford, S. K. Korotky, and R. C. Alferness, "Low-loss $Ti:LiNbO_3$ waveguide bends at $\lambda = 1.3$ μm," *IEEE Trans. Microwave Theory Tech.*, vol. MTT-30, no. 10, pp. 1790–1794, Oct. 1982.
[29] J.-P. Weber, "Spectral characteristics of coupled-waveguide Bragg-reflection tunable optical filter," *Proc. Inst. Elec. Eng.*, pt. J, vol. 140, no. 5, pp. 275–284, Oct. 1993.
[30] T. Erdogan, "Fiber grating spectra," *J. Lightwave Technol.*, vol. 15, no. 8, pp. 1277–1294, Aug. 1997.
[31] W. H. Loh, M. J. Cole, M. N. Zervas, S. Barcelos, and R. I. Laming, "Complex grating structures with uniform phase masks based on the moving fiber-scanning technique," *Opt. Lett.*, vol. 20, no. 20, pp. 2051–2053, Oct. 1995.
[32] S. J. Hewlett, J. D. Love, G. Meltz, T. J. Bailey, and W. W. Morey, "Cladding-mode coupling characteristics of Bragg gratings in depressed-cladding fiber," *Electron. Lett.*, vol. 31, no. 10, pp. 820–822, May 1995.
[33] T. Erdogan and J. E. Sipe, "Tilted fiber phase gratings," *J. Opt. Soc. Amer. A, Opt. Image Sci.*, vol. 13, no. 2, pp. 296–313, Feb. 1996.
[34] R. Feced, M. N. Zervas, and M. A. Muriel, "An efficient inverse scattering algorithm for the design of nonuniform fiber Bragg gratings," *IEEE J. Quantum Electron.*, vol. 35, no. 8, pp. 1105–1115, Aug. 1999.
[35] D. L. Lee, *Electromagnetic Principles of Integrated Optics*: Wiley, 1986, pp. 78–81.

Christos Riziotis was born on December 24, 1970, in Farsala, Greece. He received the B.S. degree in physics in 1993 and the M.Sc. degree in electronics and telecommunications in 1995, both from the National and Capodistrian University of Athens, Greece. He is currently pursuing the Ph.D. degree at the Optoelectronics Research Centre (ORC), University of Southampton, U.K.

From 1995 to 1997, he was in Hellenic Army Aviation. Since October 1997, he has been with the ORC, University of Southampton. His research interests include fabrication of photosensitive planar waveguides using Flame Hydrolysis Deposition, modeling and fabrication of waveguide and grating-based structures, and also Optical Communication systems. Currently, he is a Research Fellow in the ORC, involved on fabrication and characterization of all UV-written devices for WDM transmission systems.

Mikhail N. Zervas was born in Dimaina-Nafplias, Greece, in 1959. He received the B.S. degree in electrical engineering from Aristotle University of Thessaloniki, Greece, in 1983, the M.Sc. degree in applied and modern optics (with distinction) from the University of Reading, U.K., in 1985, and the Ph.D. degree in fiber optics from University College, London, U.K., in 1989.

In 1990, he was appointed Lecturer in the Faculty of Electrical Engineering, University of Thessaloniki. In 1991, he joined the Optoelectronics Research Centre (ORC), University of Southampton, Southampton, U.K., as a Research Fellow. In 1995, he was appointed Research Lecturer in the ORC and Electronics and Computer Science Department (ECS), University of Southampton. In 1999, he was appointed Professor in Optical Communications within the ORC/ECS. Since May 2000, he has also been with Southampton Photonics, Ltd., U.K. His main research interests are in the areas of erbium-doped fiber amplifiers, dispersion compensation, fiber, and waveguide gratings, distributed feedback fiber lasers, WDM devices, surface-plasmon-polaritons, and optical trapping. He is the author and coauthor of over 140 technical publications and 20 patents/patent applications.

Dr. Zervas has served as a member of program committees of various international conferences. He was the general Co-Chair at the 1999 Optical Amplifiers Meeting and Their Applications (OSA). In 1996, he shared a prize on "Metrology for World Class Manufacturing Awards" for his contribution on the development of a high-accuracy fiber grating characterization system.

Authorized licensed use limited to: UNIVERSITY OF SOUTHAMPTON. Downloaded on October 7, 2009 at 07:15 from IEEE Xplore. Restrictions apply.